Metallophysics and Advanced Technologies
Металофіз. новітні технол.
Metallofiz. Noveishie Tekhnol.
2021, vol. 43, No. 8, pp. 1045–1052
https://doi.org/10.15407/mfint.43.08.1045
Reprints available directly from the publisher

PACS numbers: 61.05.cp, 64.60.My, 68.35.Dv, 81.20.Ev

Influence of Carbon and Scandium on Structure of Metastable Al_3Mg Phase and Properties of SPS-Composites

A. D. Rud, A. M. Lakhnik, I. M. Kirian, O. N. Syzonenko*, N. S. Prystash*, S. O. Demchenkov**, and Yu. V. Lepeeva

G. V. Kurdyumov Institute for Metal Physics, N.A.S. of Ukraine,
36 Academician Vernadsky Blvd.,
UA-03142 Kyiv, Ukraine
**Institute of Pulse Processes and Technologies, N.A.S. of Ukraine,*
43A Bohoyavlensky Ave.,
UA-54018 Mykolaiv, Ukraine
***E. O. Paton Electric Welding Institute, N.A.S. of Ukraine,*
11 Kazymyr Malevych Str.,
UA-03150 Kyiv, Ukraine

The solid dispersant (graphite) and additional alloying by scandium effects on the intermetallic compound formation in the Al–Mg system under mechanical alloying are studied. As found, the scandium additive significantly accelerates the metastable intermetallic Al_3Mg phase formation in (75% at. (Al + 2% wt. Sc)–25% at. Mg)/5% wt. C powder mixture compared to the (75% at. Al–25% at. Mg)/5% wt. C one. The synthesized powder composite, containing metastable Al_3Mg phase and solid solution based on aluminium, is consolidated by the spark plasma sintering (SPS) method. The phase composition, structure, and hardness of the SPS sintered samples are determined by X-ray diffraction, scanning electron microscopy, and indentation by the Vickers indenter. The hardness of samples formed after spark plasma sintering is in the range of 175–212 *HV* and significantly exceeds the hardness of duralumin (124 *HV*).

Key words: aluminium-magnesium alloys, metastable Al_3Mg intermetallic compound, mechanical alloying, spark plasma sintering (SPS).

Corresponding author: Oleksandr Dmytrovych Rud'
E-mail: rud@imp.kiev.ua

Citation: A. D. Rud, A. M. Lakhnik, I. M. Kirian, O. N. Syzonenko, N. S. Prystash, S. O. Demchenkov, and Yu. V. Lepeeva, Influence of Carbon and Scandium on Structure of Metastable Al_3Mg Phase and Properties of SPS-Composites, *Metallofiz. Noveishie Tekhnol.*, **43**, No. 8: 1045–1052 (2021), DOI: 10.15407/mfint.43.08.1045.

Досліджено вплив твердофазного дисперганту (графіту) і додаткового леґування алюмінію скандієм на процес формування інтерметалічних сполук в системі Al–Mg в умовах механохемічного синтезу. Встановлено, що у разі додаткового леґування системи скандієм спостерігається значне пришвидшення процесу формування метастабільної інтерметалідної фази Al_3Mg в системі (75% ат. (Al + 2% ваг. Sc)–25% ат. Mg)/5% ваг. C порівняно із системою (75% ат. Al–25% ат. Mg)/5% ваг. C. Проведено експерименти з консолідації методом іскро-плазмового спікання синтезованого порошкового композиту, який містить метастабільну Al_3Mg-фазу та твердий розчин на основі алюмінію. Методами рентґенівської дифрактометрії, сканувальної електронної мікроскопії та індентування індентором Віккерса визначено фазовий склад, структура і твердість одержаних зразків. Встановлено, що твердість компактних зразків після іскро-плазмового спікання знаходиться в діапазоні 175–212 *HV* і значно перевищує аналогічний показник для дюралюмінію — 124 *HV*.

Ключові слова: алюміній-магнієві стопи, метастабільна інтерметалідна Al_3Mg-фаза, механічне леґування, іскро-плазмове спікання (ІПС).

(Received April 13, 2021; in final version, June 14, 2021)

1. INTRODUCTION

The rapid development of industry needs new materials with improved mechanical and operational characteristics. Due to a combination of the exclusive characteristics (lightweight, high strength, corrosion resistance, *etc.*), aluminium-magnesium alloys are largely applied in the aerospace, automotive, and transportation industries [1–3]. However, the mechanical properties of these alloys sharply degrade at high temperatures. One of the most promising options for improving the properties of Al–Mg alloys is additional alloying. It has been found, Sc induces the most strengthening effect in Al–Mg alloys. Even a small percentage of Sc results in high strength, good corrosion resistance, weldability, fatigue resistance, *etc.* [4–6] for the Al–Mg alloys.

The improvement of the mechanical properties of the Al–Mg alloys during aging is directly caused by the Guinier–Preston (GP) zones and metastable β″- and β′-phases [7–10]. The strengthening of the Al–Mg alloys is induced mainly by the metastable β″- (Al_3Mg) phase precipitation over artificial aging. This metastable β″-phase has an $L1_2$ crystalline structure. The precipitates of the metastable β″-phase are coherent to the aluminium matrix, also. It is found when the Mg percentage in the Al–Mg alloys is exceeded 20% at. the β″- (Al_3Mg) phase formed only, GP zones are not distinguished [11, 12]. The results of the Monte-Carlo atomistic simulation performed under the cluster expansion formalism for three phases (f.c.c., h.c.p., γ-phase) of the Al–Mg phase diagram and GP zones initial clustering are presented in [13]. Kleiven [13] simulated the metastable Al–Mg phase diagram and calculated the

dissolution temperatures of GP zones. The experimental data published early by [14–16] have also been analysed. The simulations suggest that GP zones are stable at slightly higher temperatures (~ 50 K) than detected in experiments.

However, conventional alloying methods are mostly exhausted and do not provide achieve the required properties of the Al–Mg alloys. Among non-equilibrium processing methods, melt-spinning [17] and mechanical alloying (MA) are extensively used to produce metastable materials [18, 19]. The control of MA parameters (deposited specific energy, milling time, ball-to-powder mass ratio, *etc.*) allows developing the synthesis modes for every specific powder system. This approach can be extended to the synthesis of the metastable intermetallic phases also, including β″-(Al_3Mg) phase, which is the main strengthening one for the Al–Mg system. It is well known the solubility of Mg in Al at room temperature is quite low and does not exceed 1% at. [20]. The mechanical alloying can significantly extend the region of magnesium solubility in the aluminium up to 45% at. [19, 21, 22]. To improve the mechanical alloying process, a wide range of surface-active additives are used. Mostly, these are liquid organic substances [23, 24]. The graphite, molybdenum disulphide, and tungsten disulphide powders are used as solid-state process control agents also.

The materials obtained by mechanical alloying are in powder form. For further research and application in the industry, it is necessary to consolidate them. Most consolidation methods require high temperatures, which can adversely affect the properties of the obtained samples. Therefore, the task of researchers is to choose a careful method of consolidation. The compaction must take place at low temperatures and short time. The spark plasma sintering (SPS) method satisfies to characteristics pointed above [25].

This article has aimed an investigating the metastable Al_3Mg phase formation in the Al–Mg and Al–Mg–Sc systems under MA in the ball mill. The 5% wt. of graphite powder is added as a process control agent. The spark plasma sintering technique is used to obtain pellets from milled powders.

2. MATERIALS AND METHODS

Commercially available powders of magnesium, spectroscopic graphite, and aluminium-scandium ligature powder are used as the starting materials. Scandium percentage in the aluminium ligature is 2% wt. Preliminarily the two initial powder mixtures are prepared: (75% at. Al–25% at. Mg)/5% wt. C and (75% at. (Al + 2% wt. Sc)–25% at. Mg)/5% wt. C. The mechanical alloying performed on a high-energy laboratory planetary ball mill (Fritsch Pulverisette P-6) at room temperature in a stainless steel vessel under the argon atmosphere. The

rotation speed of the grinding container and ball-to-powder ratio is 400 rpm and 15:1 during all experiments, respectively.

Consolidation of the MA powder is performed by the SPS technique on the 'Gefest-10' homemade experimental device, constructed at the Institute of Pulse Processes and Technologies of the National Academy of Sciences of Ukraine. Before the sintering, we put 3 g of the powder into the cylindrical graphite crucible (made of MPG-6 graphite [26]) of 10 mm in inner diameter. The sintering temperature (500 and 600°C), the value of pre-pressing pressure (~ 30 MPa), and the sintering pressure (~45 MPa) are the same in all experiments.

The phase analysis of the samples is performed by the XRD method. X-ray diffraction patterns are recorded using a powder diffractometer (HZG-4A) in the Bragg–Brentano geometry with radiations CoK_α and CuK_α. The XRD patterns are analysed using MAUD software [27]. Scanning electron microscopes studies of the sintered composite are performed on a JEOL JSEM IT-500 microscope. The hardness measurement is done using a Vickers indentation device on the polished surface of the composite sample. Measurements are carried out at a load of 49 N at room temperature.

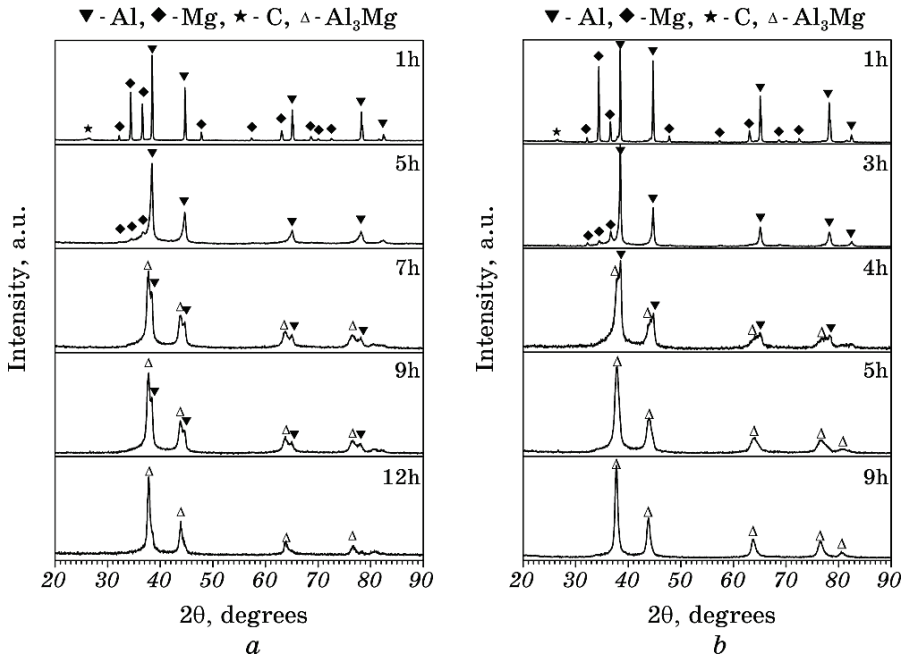

Fig. 1. The X-diffraction patterns of powder mixture after milling: (75% at. Al–25% at. Mg)/5% wt. C (*a*), (75% at. (Al + 2% wt. Sc)–25% at. Mg)/5% wt. C (*b*), radiation CuK_α.

3. RESULTS AND DISCUSSION

XRD patterns for the powder mixture (75% at. Al–25% at. Mg)/5% wt. C before and after milling are in Fig. 1, *a*. There are no additional phases in the powder mixture after 1 hour milling (see Fig. 1). The identified sharp peaks are attributed to Al, Mg, and graphite phases only. The peaks related to graphite and magnesium on the XRD diffraction pattern after 5 hours of grinding almost completely disappeared. The broadening of the Al peaks after MA for 5 hours is caused by a decrease in the crystallite size and distortion of the crystalline lattice, which indicates the reaction between Al and Mg. The peaks related to the f.c.c. Al on XRD pattern have split into two ones, associated with the Al_3Mg phase and Al-based solid solution (Fig. 1, *a*, 7 hours), respectively. The lattice parameters calculated for these two diffraction peaks are 0.4119 nm and 0.4048 nm, respectively. Further MA to 9 hours and 12 hours does not alter the phase composition but results in an increase in the volume of the metastable intermetallic Al_3Mg phase. The best Rietveld refinement for XRD pattern after MA 12 hours is obtained for two phases: Al_3Mg—79.2% wt. and Al-based solid solution—20.8% wt. The lattice parameters for these phases are 0.4123 nm and 0.4057 nm, respectively. The obtained unit cell parameter for the Al_3Mg intermetallic compound is in good agreement with the experimental (0.413 nm) [28] and calculated (0.412 nm) [29, 30] data. The presence of the intermetallic Al_3Mg phase in the sample (75% at. Al–25% at. Mg)/5% wt. C after 12 hours MA processing is also confirmed by electron microdiffraction [31].

The influence of Sc on the evolution of phase composition in the

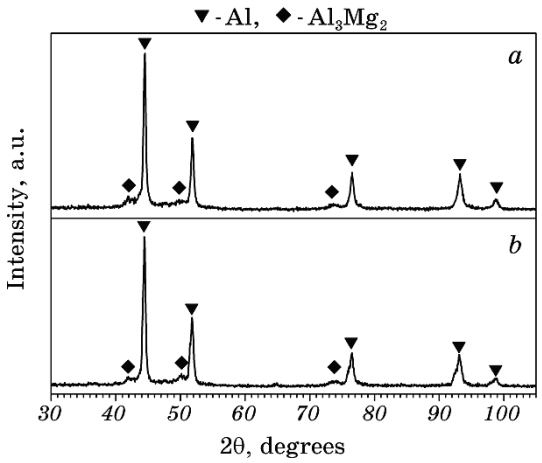

Fig. 2. XRD patterns of the SPS sintered composites at a different temperatures: 500°C (*a*), 600°C (*b*), radiation CoK_α.

(75% at. (Al + 2% wt. Sc)–25% at. Mg)/5% wt. C powder mixture under MA are shown in Fig. 1, *b*. The 1 hour MA has no obvious effect on the phase composition. Phase analysis found that on the X-Ray patterns are only present peaks typical for aluminium, magnesium, and carbon.

After 3 hours of MA, the intensity of peaks associated with Mg decreases. After 4 hours of MA, the Mg peaks disappeared. According to the XRD phase analysis, there are two phases: Al_3Mg ~ 40% wt. and aluminium ~60% wt. in the powder after 4 hours of MA. The Rietveld refinement for XRD patterns after MA 5 hours is obtained for the f.c.c. Al(Mg) solid solution and metastable intermetallic Al_3Mg phase with $L1_2$ crystal structure type. The cell parameters for Al-based solid solution and Al_3Mg phases are 0.4091 nm and 0.4128 nm, respectively. Further MA during 9 hours does not vary the phase composition of the sample, but increases the amount of the metastable intermetallic Al3Mg phase. The best Rietveld refinement for XRD pattern after MA 9 hours is achieved for two phases: Al(Mg)-solid solution and Al_3Mg—(the lattice parameters are 0.4066 nm and 0.4112 nm, respectively). Analysing the processes occurring during the mechanical alloying of powder mixture (75% at. (Al + 2% wt. Sc)–25% at. Mg)/5% wt. C, we should note a significant acceleration of the processes of phase formation and a change in the phase composition in contrast to (75% at. Al–25% at. Mg)/5% wt. C. Therefore, the simultaneous alloying of aluminium by scandium and the use of graphite powder as a solid-state process control agent markedly favour the metastable intermetallic Al_3Mg phase formation. The composite, synthesized by the MA 9 hours of the powder mixture (75% at. (Al + 2% wt. Sc)–25% at. Mg)/5% wt. C is consolidated by the spark plasma sintering method at 500 and 600°C. The XRD patterns recorded for sintered samples are shown in Fig. 2.

The XRD patterns exhibit weak diffraction peaks at ~42, 50, and 73° (2θ). The low-intensity peaks associated with the Al_3Mg_2 phase. The

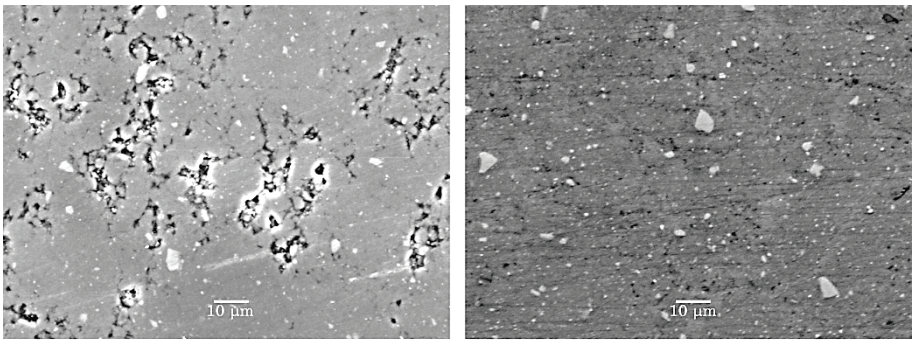

a *b*

Fig. 3. Microstructure of SPS sintered composites at 500°C (*a*) and 600°C (*b*).

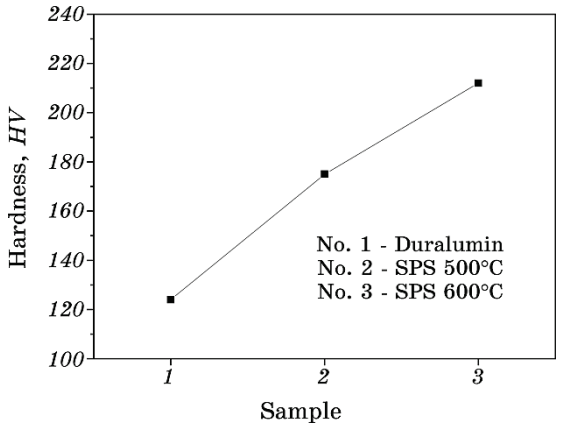

Fig. 4. Vickers hardness of duralumin and SPS-sintered samples.

high-intensity peaks are related to f.c.c. Al solid solution. The lattice parameter of the f.c.c. Al phase increases from 0.4092 nm to 0.4098 nm. Perhaps it is caused by the formation of a more oversaturated f.c.c. Al solid solution after SPS at the 600°C, in contrast, to the sample sintered at the 500°C.

The SEM electron images taken from the polished surface cross-section composites sintered at different temperatures are shown in Fig. 3. It is quite clear, the higher porosity is in the sample sintered at 500°C in contrast to the sample sintered at 600°C.

Vickers hardness values measured on the SPS sintered samples and duralumin as an etalon sample is presented in Fig. 4. The measured hardness for duralumin is 124 *HV*. The hardness for the sample sintered at 500°C is 175 *HV*. The increase in the sintering temperature to 600°C results in a growth in the hardness up to ~212 *HV*.

4. CONCLUSION

Mechanical alloying by high-energy ball milling is successfully used to produce metastable intermetallic Al_3Mg phase having $L1_2$ crystal structure type. It is found, additional alloying by scandium accelerates the process of Al_3Mg phase formation in the (75% at. Al–25% at. Mg)/5% wt. C powder mixture. Bulk composite materials based on the Al_3Mg phase are fabricated using a spark plasma sintering technique. The Vickers hardness values for SPS sintered pellets are more than twice as high as that of duralumin.

This work is supported by budget theme No. 025/21 of the G. V. Kurdyumov Institute for Metal Physics, N.A.S. of Ukraine and the youth project of the National Academy of Sciences of Ukraine

No. 06/01-2021(03).

REFERENCES

1. A. Jambor and M. Beyer, *Materials and Design*, **18**: 203 (1997).
2. D. R. Lesuer and G. J. Kipouros, *JOM*, **47**: 17 (1995).
3. J. E. Allison and G. S. Cole, *JOM*, **45**: 19 (1993).
4. Z. Yin, Q. Pan, Y. Zhang, and F. Jiang, *Mater. Sci. Eng. A*, **280**, Iss. 1: 151 (2000).
5. A. L. Berezina, T. A. Monastyrskaya, E. A. Segida, K. V. Chuistov, U. Shmidt, and A. V. Kotko, *Engineering Mechanics*, **11**, No. 5: 393 (2004).
6. Yu. A. Filatov, V. I. Yelagin, and V. V. Zakharov, *Mater. Sci. Eng. A*, **280**, Iss. 1: 97 (2000).
7. M. Bouchear, D. Hamana, and T. Laout, *Phil. Mag. A*, **73**: 1733 (1996).
8. M. J. Starink and A-M. Zahra, *Acta Mater.*, **46**, 10: 3381 (1998).
9. D. Hamana, M. Bouchear, M. Betrouche, A. Derafa, and N. Y. Rokhmanov, *J. Alloys Compd.*, **320**: 93 (2001).
10. M. Slámová, M. Janeček, and M. Cieslar, *Mater. Sci. Eng. A*, **462**: 375 (2007).
11. Yi. Gaosong, D. A. Cullen, K. C. Littrell, W. Golumbfskie, E. Sundberg, and M. L. Free, *Metall. Mater. Trans. A*, **48**: 2040 (2017).
12. T. Sato and A. Kamio, *Mater. Sci. Eng. A*, **146**, Iss. 1–2: 161 (1991).
13. D. Kleiven, O. L. Ødegård, K. Laasonen, and J. Akola, *Acta Mater.*, **166**: 484 (2019).
14. T. Sato, Y. Kojima, and T. Takahashi, *Metall. Mater. Trans. A*, **13**: 1373 (1982).
15. K. Osamura and T. Ogura, *Metall. Mater. Trans. A*, **15**: 835 (1984).
16. C. Gault, A. Dauger, and P. Boch, *Acta Mater.*, **28**, Iss. 1: 51 (1980).
17. A. L. Berezina, E. A. Segida, T. A. Monastyrskaya, and A. V. Kotko, *Metallofiz. Noveishie Tekhnol.*, **30**, No. 6: 849 (2008) (in Russian).
18. J. S. Benjamin, *Sci. American*, **234**: 40 (1976).
19. D. L. Zhang, T. B. Massalski, and M. R. Paruchuri, *Metall. Mater. Trans. A*, **25**: 73 (1994).
20. C. Vargel, *Corrosion of Aluminium* (Elsevier: 2004), p. 211.
21. A. Calka, W. Kaczmarek, and J. S. Williams, *J. Mater. Sci.*, **28**: 15 (1993).
22. M. Schoenitz and E. L. Dreizin, *J. Mater. Res.*, **18**: 1827 (2003).
23. L. Liu and Y. F. Zhang, *J. Alloys Compd.*, **290**, Iss. 1–2: 279 (1999).
24. S. A. Rounaghi and E. Esmaeili, *J. Nanostruct.*, **7**, Iss. 2: 147 (2017).
25. Z. A. Munir, D. V. Quach, and M. Ohyanagi, *J. Am. Ceram. Soc.*, **94**: 1 (2011).
26. O. N. Sizonenko, E. G. Grigoryev, N. S. Pristash, A. D. Zaichenko, A. S. Torpakov, Ye. V. Lypian, V. A. Tregub, A. G. Zholnin, A. V. Yudin, and A. A. Kovalenko, *High Temp. Mater. Process.*, **36**, Iss. 9: 891 (2017).
27. L. Luterotti and S. Gialanella, *Acta Mater.*, **46**, Iss. 1: 101 (1998).
28. A. F. Norman, P. B. Prangell, and R. S. McEwen, *Acta Mater.*, **46**, Iss. 16: 5715 (1999).
29. R. Yang, B. Tang, and T. Gao, *Int. J. Modern Phys. B*, **30**, No. 01: 1550243 (2017).
30. D.-L. Li, P. Chen, J.-X. Yi, B.-Y. Tang, L.-M. Peng, and W.-J. Ding, *J. Phys. D: Appl. Phys.*, **42**: 225407 (2009).
31. A. D. Rud, I. M. Kirian, A. M. Lakhnik, A. V. Kotko, and N. D. Rud, *Appl. Nanosci.* (2021).